JOURNAL OF AIRCRAFT
Vol. 47, No. 4, July–August 2010

Effect of Normal Blowing on Compressible Convex-Corner Flows

Kung-Ming Chung*
National Cheng-Kung University, Tainan 701, Taiwan, Republic of China

DOI: 10.2514/1.46889

An experimental program was conducted to investigate the upstream blowing rate and air-injection pattern on compressible convex-corner flows. The upstream normal blowing jet tends to decrease the local Mach number, the adverse pressure gradient downstream of the corner, and the peak pressure fluctuations in subsonic interactions. This results in a delay in transition of subsonic and transonic expansion flows. Upstream movement of shock waves in transonic interactions is coupled with the shock oscillation and a higher level of downstream surface-pressure fluctuations. The effect of the air-injection pattern is more pronounced on the intensity of peak pressure fluctuations.

Nomenclature

A_j	=	area of all injection holes, cm^2
$A_{j\text{-dis}}$	=	area of rectangle that contains all injection holes, cm^2
B_d	=	blowing parameter
C_p	=	pressure coefficient, $(p_w - p_\infty)/q_\infty$
C_{σ_p}	=	pressure fluctuation coefficient, $(\sigma_{p,w} - \sigma_{p,\infty})/q_\infty$
M	=	freestream Mach number
M_1	=	local Mach number upstream of shock
p_∞, p_w	=	mean surface static pressure
q_∞	=	freestream dynamic pressure
x	=	coordinate along the surface of the corner, cm
x^*	=	normalized streamwise distance, x/δ
X_i^*	=	region of separated boundary layer
X_{sep}^*	=	shock location
β	=	similarity parameter, $M^2\eta/\sqrt{1-M^2}$
δ	=	incoming boundary-layer thickness, mm
η	=	convex-corner angle, deg
σ_p	=	surface-pressure fluctuation
ϕ	=	porosity, $A_j/A_{j\text{-dis}}$

I. Introduction

DEFLECTED flaps at cruise and nonstandard flight conditions can be used as a high-lift device to obtain the maximum performance of an aircraft [1]. In particular, the case of subsonic and transonic flow suddenly expanding around a corner and then recompressing is critical for the study of external aerodynamics on both fighter and transport aircraft [2]. Chung [3] indicated that a compressible convex-corner flow shows a mild initial expansion, a strong expansion near the corner, and downstream recompression. Transition of the subsonic and transonic expansion flow and the interaction region can be scaled with the freestream Mach number and the convex-corner angle ($M^2\eta$), and a small separation bubble may be borne at the formation of a normal shock wave [4]. With an increasing convex-corner angle, the separation position moves slightly upstream, while the reattachment position moves downstream. An extensively shock-induced separated region is observed at $M^2\eta \geq 8.95$ [5]. In addition, the measurements of surface-pressure fluctuations indicate the intermittent nature of the pressure signals, and the intensity of peak pressure fluctuations could also be scaled with $M^2\eta$. The unsteadiness of the flow is related to the type of expansion flow and shock oscillation.

The influence of disturbances originating in the incoming boundary layer is of interest for flow unsteadiness. Artificial disturbances can be introduced into the flow through air injection. It is known that even a small quantity of high-pressure air can energize and alter the shape of the incoming boundary layer, thus inducing the increase in displacement thickness (or decreasing Reynolds number). By injecting air through a porous plate, and by changing the blowing rate, the fullness of the boundary-layer profile can easily be reduced, and the boundary layer becomes thicker at the same time. Inger and Zee [6] further indicated that the effectiveness of blowing is related to the rates of injection. Lower mass injections produce only modest effects on the boundary-layer profile or the freestream flow, while very large rates of injection may cause separation of the injected mass and the boundary layer [7]. Furthermore, the organized motion in the incoming boundary layer has a dramatic effect on shock unsteadiness. The intensity of pressure fluctuations and the amplitude of the shock motion might increase substantially with upstream artificial disturbances [8]. For the effect of normal blowing on convex-corner flows, a preliminary study was conducted by Chung [9]. Two porous plates (1.0 and 2.0 mm in diameter) with 82 uniformly distributed normal holes were installed upstream of the corner. The intensity of the surface-pressure fluctuations and the transition of subsonic and transonic expansion corner flows are associated with the upstream blowing rates. To further clarify the effect of normal blowing jet, tests were made using a series of air-injection patterns on subsonic and transonic convex-corner flows. The aim of the present work was to make a systematic study of this upstream normal blowing jet effect. The analysis of mean and fluctuating pressure distributions was conducted to evaluate the blowing rate and air-injection pattern on pressure distribution and fluctuating pressure load.

II. Experimental Techniques

A. Transonic Wind Tunnel

The Aerospace Science and Technology Research Center/National Cheng-Kung University (ASTRC/NCKU) transonic wind tunnel is a blowdown type, and it can be operated from Mach 0.2 to 1.4, at Reynolds numbers up to 20 million per meter [10]. Major components of the facility include compressors, air dryers, a cooling water system, storage tanks, and a tunnel. The dew point of the high-pressure air through the dryers is maintained at −40°C under normal operating conditions. Air storage volume for the three storage tanks is up to 180 m^3 at 5.15 MPa. The test section is 600 × 600 mm and 1500 mm long. In the present study, the test section has a combination of solid sidewalls and perforated top/bottom walls, in which the tunnel background acoustic noise is lower in comparison with that of perforated sidewalls. The freestream Mach numbers were 0.64 and 0.83 ± 0.01. The stagnation pressure p_o and temperature T_o were 172 ± 0.5 kPa and ambient temperature, respectively.

Presented as Paper 2008-6409 at the 26th AIAA Applied Aerodynamics Conference, Honolulu, HI, 18–21 August 2008; received 26 August 2009; revision received 22 April 2010; accepted for publication 23 April 2010.

*Research Fellow, Aerospace Science and Technology Research Center. Senior Member AIAA.

For the data acquisition system, the test conditions were recorded by the NEFF system, while LeCroy 6810 waveform recorders were used for the pressure measurements. A host computer with Catalyst software controlled the setup of the LeCroy waveform recorders through a LeCroy 8901A interface. All input channels were triggered simultaneously, using an input channel as the trigger source. The output range of waveform recorders was adjusted for an optimum resolution, and the relative error of the mean pressure signals was estimated to be about 0.1%.

B. Testing Models

The test model consists of a flat plate, a perforated plate, and an interchangeable instrumentation plate, as shown in Fig. 1a. The test model is 150 mm wide and 600 mm long, and it is supported by a single sting mounted on the bottom wall of the test section. The high-pressure air was injected through the perforated plate, as seen in Fig. 1b. The plates had uniformly distributed normal holes, with diameters of 1.5 mm, and the holes were uniformly distributed in four rows and in a pattern symmetric with the centerline. The last row was located 7 mm upstream of the convex corner. The blowing jet was supplied from a plenum underneath, connected to the high-pressure air tank through an 8 mm pipe. The 13, 15, or 17 deg convex corner was located at 500 mm from the leading edge of the flat plate. Ten flush-mounted pressure transducers were installed along the centerline of each instrumentation plate, perpendicular to the test surface. Side fences were installed on the instrumentation plate to prevent crossflow from the underside of the plate. The oil-flow visualization was also applied to ensure two-dimensional flow.

C. Experimental Technique

The Kulite (model XCS-093-25A, B screen) pressure transducers were powered by a Topward Electronic System (TES model 6102) power supply at 15.0 V. The outer diameter was 2.36 mm, and the sensing element was 0.97 mm in diameter. External amplifiers (Ecreon model E713) were also employed to improve the signal-to-noise ratio. The natural frequency of the Kulite pressure transducers is 200 kHz, as quoted by the manufacturer. However, Gramann and Dolling [11] indicated that the perforated screen of the transducers might limit the frequency response only up to 50 kHz. The sampling period is 5 μs (200 kHz) for all the test cases. Each data record contains 131,072 data points for statistical analysis. The data were divided into 32 blocks. The mean values of each block (4096 data points) were calculated. Uncertainty of the experimental data of the flat plate case was estimated to be 0.43 and 0.15% for the static pressure coefficient and surface-pressure fluctuation coefficient, respectively. For the characteristics of the incoming boundary layer, Miau et al. [12] indicated that the transition of the boundary layer under the present test condition is close to the leading edge of the flat plate. The boundary-layer thicknesses, in the absence of the perforated plate, at 25 mm upstream of the convex corner, were estimated to be 7.3 and 7.1 ± 0.2 mm for $M = 0.64$ and 0.83, respectively. The Reynolds numbers based on the incoming boundary-layer thickness Re_δ were 1.49 and 1.68×10^5, respectively.

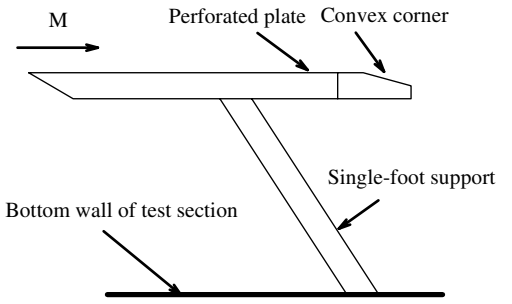

a) Test model

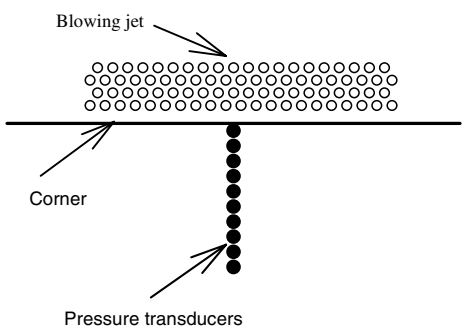

b) Instrumentation plate

Fig. 1 Test configuration.

Table 1 Configuration of perforated plates (1.5 mm in diameter).

Plate	$A_{j\text{-dis}}$, cm^2	Injection holes (1.5 mm in diameter)	ϕ, %
1	3.1×10.1	82	4.63
2	3.1×10.1	104	5.87
3	3.1×10.1	144	8.13
4	1.6×10.1	82	8.97

A 4 mm sonic nozzle, manufactured by Flow Systems, was installed to control the mass flow of the blowing jet. The rates of blowing were calculated according to the stagnation condition upstream of the sonic nozzle (Kulite pressure transducer model XT-140-500A) and the temperature of the high-pressure air tank. The stagnation pressure $p_{o,j}$ ranged from 0.3 to 1.0 MPa, and the stagnation temperature was ambient temperature. The blowing-jet-to-freestream-stagnation-pressure ratio ($p^*_{o,j} = p_{o,j}/p_o$) was up to 5.88. Injection was taking place over two-thirds of the width of the perforated plate (100 mm wide). The blowing parameter B_d was also used as a measure of nondimensional mass injection, in which

$$B_d = \frac{\rho_j U_j A_j}{\rho_\infty U_\infty A_{j\text{-dis}}}$$

where $A_{j\text{-dis}}$ is the area contained within the perimeter of a rectangle, which just circumscribes all the injection holes [13]. In the present situation, the blowing parameter B_d ranges from 0.007 to 0.052. The porosity ($A_j/A_{j\text{-dis}}$, ϕ) was from 4.63 to 8.97%, as shown in Table 1.

III. Results and Discussion

A. Mean Surface-Pressure Distributions

The flow behavior near the convex corner, as a geometric singularity, is of an expansion and recompression process, which is associated with compressibility and viscous–inviscid interaction [14]. At lower Mach numbers and moderate convex-corner angles, the expansion is of a pure subsonic case. With increasing Mach numbers and convex-corner angles, the flow expands to supersonic speed. Recompression occurs through an embedded shock wave [2]. In the present study, comprehensive measurements of surface pressure for the cases with upstream blowing jet were made downstream of the corner apex. Two groups of air-injection pattern were of interest. For case A (plates 1, 2, and 3), the perimeter of the rectangle that circumscribes all the injection holes is the same. The porosity is associated with the number of injection holes. For case B (plates 1 and 4), the number of injection holes is the same for both porous plates. The blowing parameter B_d of plate 4 at a given stagnation pressure ratio $p^*_{o,j}$ is only half of plate 1.

At $M = 0.64$ and $\eta = 13$ deg, distributions of the mean pressure coefficient C_p for case A are shown in Fig. 2. This corresponds to a typical subsonic expansion flow, where x^* denotes the nondimensional coordinate measured along the body surface from the corner apex. The results with the four injection rates are plotted together, and the test case without the upstream blowing jet (solid symbol) is

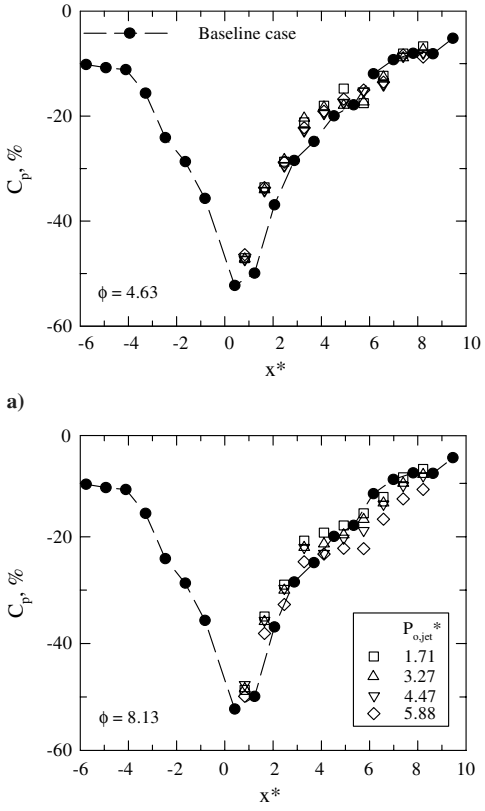

Fig. 2 Pressure distributions: $M = 0.64$, $\eta = 13$ deg.

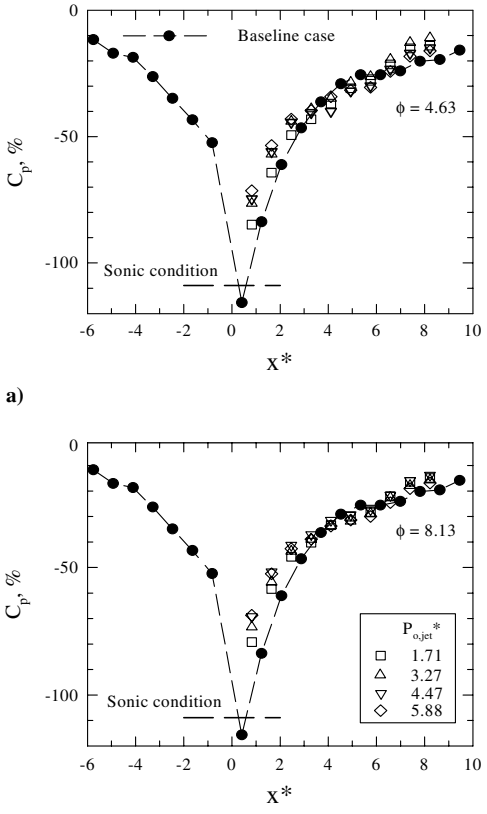

Fig. 3 Pressure distributions: $M = 0.64$, $\eta = 17$ deg.

denoted as the baseline case. With the 4.63% perforated plate, higher levels of C_p are observed up to $x^* \fallingdotseq 4$. This corresponds to less expansive flow near the corner. At further downstream locations, the upstream blowing jet does not have a marked effect on the shape of the pressure distribution. The data also show little variation with $p^*_{o,j}$ (or B_d) under these test conditions. In Fig. 2b, slightly higher C_p is also observed near the corner, with the 8.13% perforated plate. At $M = 0.64$ and $\eta = 17$ deg, the flow expanded to the supersonic speed and recompressed back to subsonic condition downstream, as seen in Fig. 3. The effect of the upstream blowing jet is limited near the corner, in which higher C_p (or lower local Mach number) is observed. This is similar to the observation by Chung [9], in which there is a delay in the transition of subsonic and transonic expansion flow. In addition, the level of C_p near the corner increases with higher $p^*_{o,j}$, and the porosity effect is not evident. The baseline case at $M = 0.83$ and $\eta = 17$ deg is a transonic expansion flow with shock-induced separation, as seen in Fig. 4. The flow expanded to sonic speed near the corner apex, and it remained at supersonic condition throughout the measurement locations. With the upstream blowing jet, the level of C_p is considerably higher than that of the baseline case, particularly for the case of $\phi = 4.63$. This is related to the upstream movement of the shock wave, and distinctive kink pressure at $x^* \fallingdotseq 2$ is associated with the shock-induced separation phenomenon. It is also noted that the effect of $p^*_{o,j}$ on the flow development downstream of the corner is similar to the test case at $M = 0.64$ and $\eta = 17$ deg with the 4.63% porous plate. For $\phi = 8.63$, the C_p distributions at four $p^*_{o,j}$ are roughly the same, except for the amplitude of kink pressure.

For case B, the rectangle, which circumscribes all the injection holes of porous plate 4, is only half of that of porous plate 1. Examples of C_p distribution are shown in Figs. 5 and 6. For the subsonic expansion flow ($M = 0.64$ and $\eta = 15$ deg), the upstream blowing jet results in considerably higher C_p near the corner apex. The level of C_p also increases slightly with higher $p^*_{o,j}$. Further downstream, the effect of the upstream blowing jet on the flow development is minimized. This is associated with less initial recompression (or adverse pressure gradient). It is also noted that the level of C_p of $\phi = 8.97$ is slightly higher than that of $\phi = 4.63$. The test case at $M = 0.83$ and $\eta = 15$ deg represents a transonic expansion flow. Upstream movement of the shock wave is not

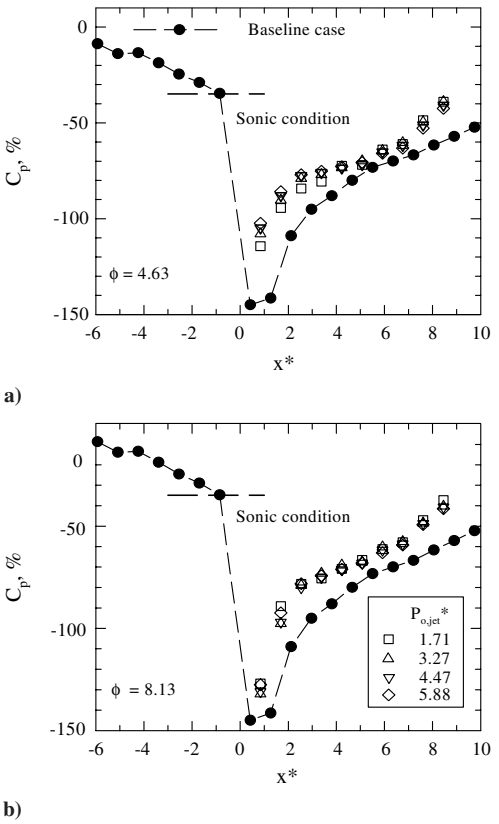

Fig. 4 Pressure distributions: $M = 0.83$, $\eta = 17$ deg.

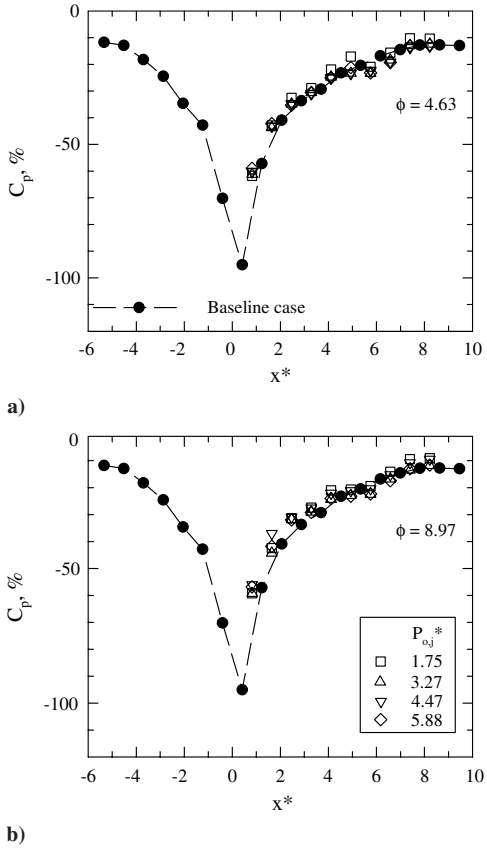

Fig. 5 Pressure distributions: $M = 0.64$, $\eta = 15$ deg.

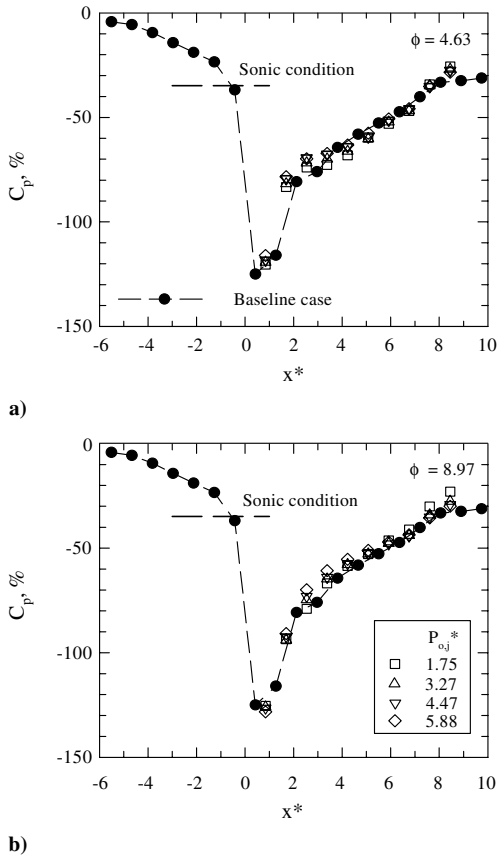

Fig. 6 Pressure distributions: $M = 0.83$, $\eta = 15$ deg.

observed, as seen in the case of $M = 0.83$ and $\eta = 17$ deg. In general, the downstream pressure distributions are not much influenced by the upstream blowing jet. However, a lower level of C_p is observed with $\phi = 8.97$. This corresponds to a higher local Mach number or stronger expansion near the corner apex.

B. Surface-Pressure Fluctuations

Distributions of surface-pressure fluctuations for a subsonic expansion flow ($M = 0.64$ and $\eta = 13$ deg) are shown in Fig. 7. The pressure fluctuation coefficient C_{σ_p} represents the local wall pressure fluctuations (rms values) normalized by the freestream dynamic pressure q_∞ with respect to undisturbed flows ($\sigma_{p,\infty}/q_\infty$). Other than the lower amplitude of C_{σ_p} near the corner apex, the distributions of surface-pressure fluctuation, with and without the upstream blowing jet, are in close agreement with each other. They also show little variation with the blowing rate. This suggests that the flow conditions away from the corner apex are virtually independent of the state of the upstream boundary layer. It is noted that the distributions of mean surface pressure (Fig. 2) show a similar trend. Furthermore, Laganelli and Martellucci [15] indicated that the amplitude of the surface-pressure fluctuation is associated with the local Mach number. With the upstream blowing jet, the reduction in C_{σ_p} near the corner apex is considered due to less expansive flow.

At $M = 0.64$ and $\eta = 17$ deg, the shock induces stronger adverse pressure gradient and intense pressure fluctuations for the baseline case. With the upstream blowing jet, it is known that the upstream blowing jet results in the delay in transition of subsonic and transonic expansion flows. This is associated with the reduction in the adverse pressure gradient downstream of the corner apex, which is shown in the mean surface-pressure distributions. Decreasing peak C_{σ_p} at higher blowing rates is observed in Fig. 8, particularly for $\phi = 8.13$. The levels of C_{σ_p} reach the equilibrium conditions quickly downstream of the corner, and they are comparably higher than that of the baseline case. For a transonic expansion flow with shock-induced separation ($M = 0.83$ and $\eta = 17$ deg, Fig. 9), it can be seen that the location of peak C_{σ_p} moves upstream. A comprehensive survey by Dolling [16] indicated that the rapid rise in surface-pressure fluctuations upstream of separation and higher downstream surface-pressure fluctuations are a common feature of many shock wave/turbulent boundary-layer interactions, in which the peak pressure fluctuations are mainly associated with the shock excursion

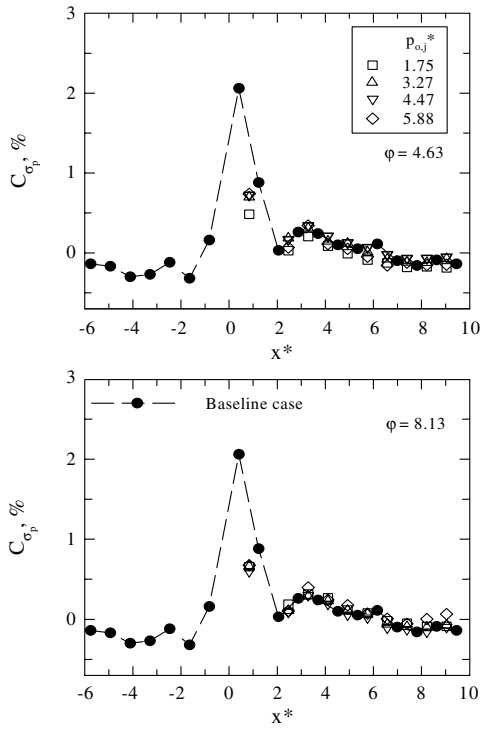

Fig. 7 Pressure fluctuations: $M = 0.64$, $\eta = 13$ deg.

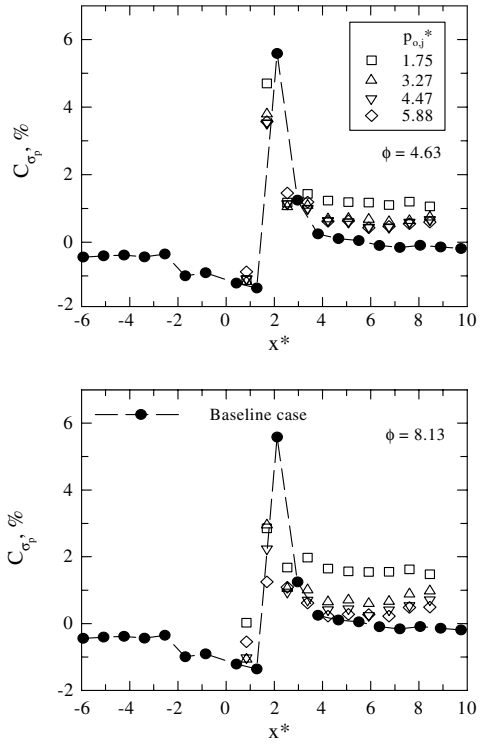

Fig. 8 Pressure fluctuations: $M = 0.64$, $\eta = 17$ deg.

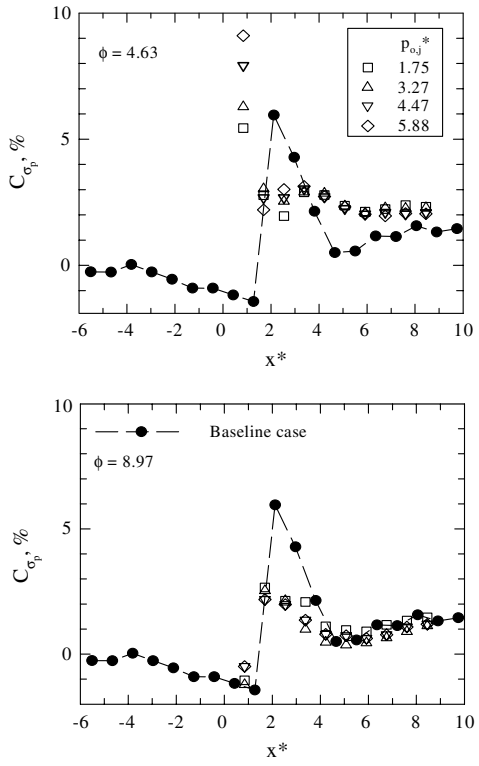

Fig. 10 Pressure fluctuations: $M = 0.83$, $\eta = 15$ deg.

phenomenon. Thus, the movement of peak surface-pressure fluctuations with an upstream blowing jet implies the expansion of a separation bubble. Stronger downstream C_{σ_p} and the minor influence of the blowing rate for the case of $\phi = 4.63$ can also be seen. For $\phi = 8.13$, the amplitude of C_{σ_p} is lower than that of $\phi = 4.63$. The downstream surface-pressure fluctuations increase slightly with a higher blowing rate.

The air-injection pattern on the surface-pressure fluctuations is of interest. In Fig. 10 ($M = 0.83$ and $\eta = 15 \cdot$ deg), the momentum ratio, $(\rho_j U_j)/(\rho_\infty U_\infty)$, at a given $p^*_{o,j}$ is the same for both test cases. However, it is intuitively thought that a smaller rectangle circumscribing all the injection holes ($\phi = 8.97$) modifies the upstream boundary-layer shape in a manner similar to the situation of higher blowing rate. The results are in close agreement with the observation from the test cases of the porous plates 1 and 3 (Fig. 9, $M = 0.83$ and $\eta = 17$ deg). Reduced fullness of upstream boundary-layer shape initially enhances the shock excursion (or peak surface-pressure fluctuation) and downstream surface-pressure

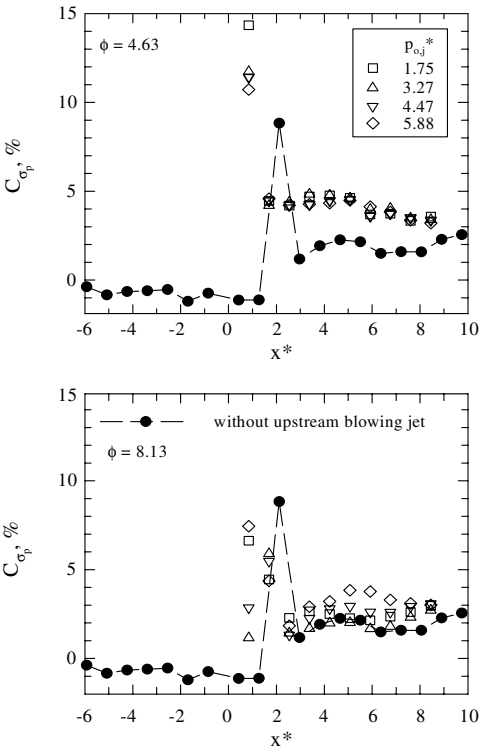

Fig. 9 Pressure fluctuations: $M = 0.83$, $\eta = 17$ deg.

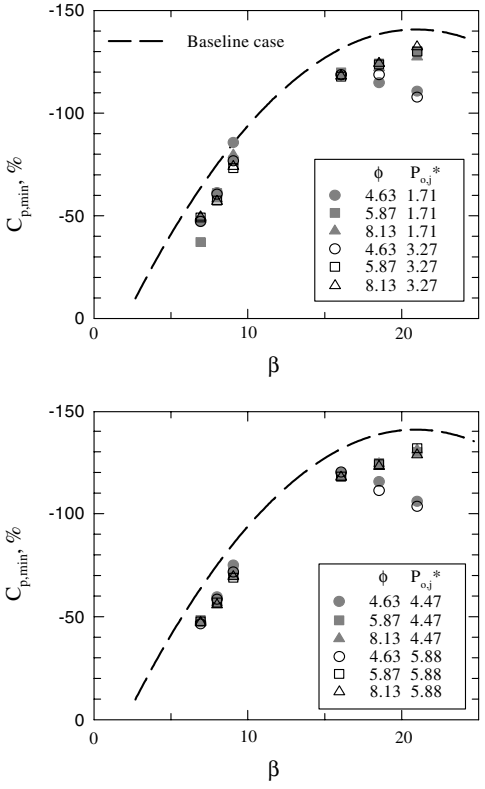

Fig. 11 Downstream expansion.

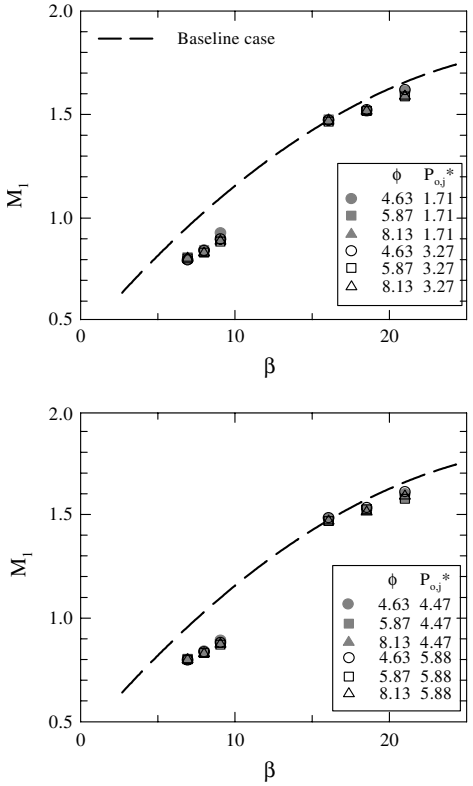

Fig. 12 Peak Mach number.

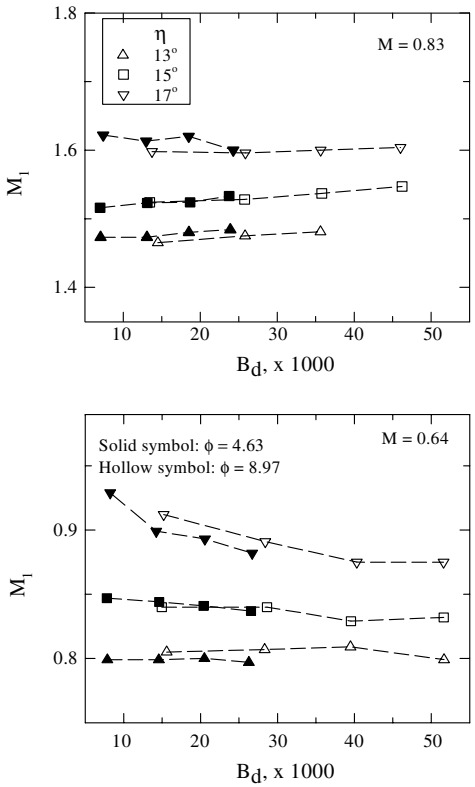

Fig. 13 Peak Mach number: B_d effect.

fluctuations ($\phi = 4.63$). With higher porosity ($\phi = 8.97$), only the surface-pressure fluctuations downstream of the corner are influenced by the upstream injection. A lower peak C_{σ_p} is observed, and there is little variation on the levels of downstream C_{σ_p}. The blowing rate on the surface-pressure fluctuations is minimized for this test case.

C. Viscous–Inviscid Interactions

Boundary-layer flow in the vicinity of a sharp corner has been investigated by many researchers, particularly for the compression corner in supersonic speed. For a convex-corner flow, it is possible to formulate the interaction law in an explicit form that would relate the displacement effect of the boundary layer to the pressure induced in the inviscid part of subsonic and supersonic flows. In transonic flow, there are not many studies that explain the flow properties as a result of the viscous–inviscid interaction near the corner point [17]. For a laminar boundary layer, Ruban and Turkyilmaz [18] indicated that the displacement effect in a convex-corner flow is primarily due to the inviscid part. The flow in the interaction region is governed by the inviscid–inviscid interaction (the main part of the boundary layer and the potential flow region outside the boundary layer), and the contribution of the viscous sublayer is negligible to the leading order. However, a subsequent study by Ruban et al. [14] pointed out that the main contribution to the displacement thickness is produced by the overlapping region that lies between the viscous sublayer and main part of the boundary layer. For a turbulent boundary layer, there is no theoretical analysis available for the transonic convex-corner flows. Another problem is the shock-induced turbulent boundary-layer separation.

The minimum mean surface pressure $C_{p,\min}$ near the corner is related to the upstream expansion and the initial downstream compression process. Chung [3] indicated that the amplitude of $C_{p,\min}$ can be scaled with the parameter $M^2\eta$. He postulates that a stronger expansion or higher peak Mach number is coupled with an increasing freestream Mach number and convex-corner angle. Furthermore, a study by Verhoff et al. [19] on compressible flow past a corner used the change of variable for a hodograph solution, in which $\beta \equiv M^2\eta/\sqrt{1-M^2}$. For the present study, results of $C_{p,\min}$ versus β are shown in Fig. 11 (case A). The dashed line represents the baseline case. In general, the upstream blowing jet results in less expansive flow for all the test cases. There is little variation with the blowing rate for subsonic expansion flow. However, the amplitude of $C_{p,\min}$ for $\phi = 4.63$ is considerably lower than those of the other two

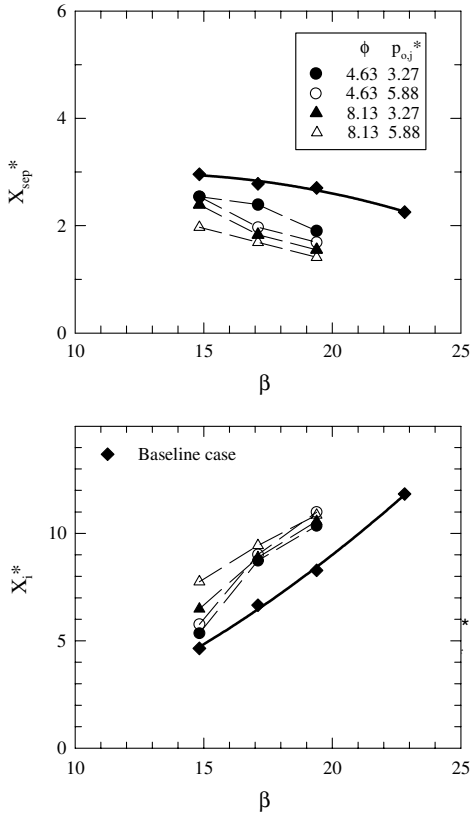

Fig. 14 Interaction region (case A).

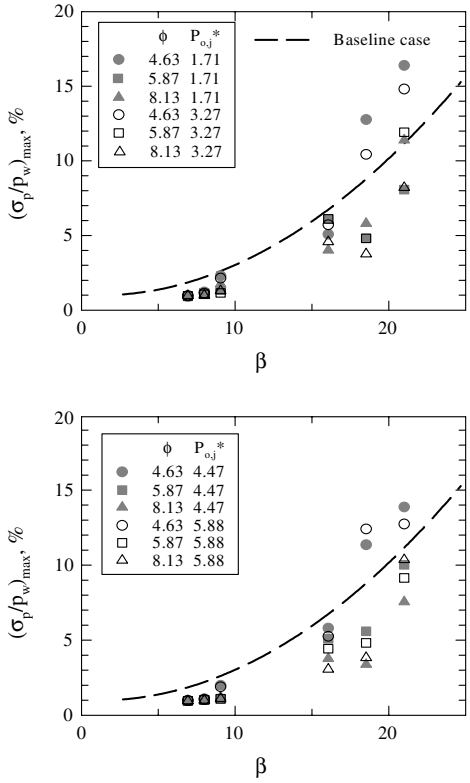

Fig. 15 Peak pressure fluctuations.

porous plates at all four blowing rates. As mentioned earlier, this corresponds to the upstream movement of the shock wave. In addition, the nature of the interaction between the shock wave and the boundary layer depends primarily on whether the local Mach number is greater than or less than some critical value [20]. Since the instantaneous wall pressure in the transonic interactions is highly intermittent, $C_{p,\min}$ does not correspond to the real local Mach

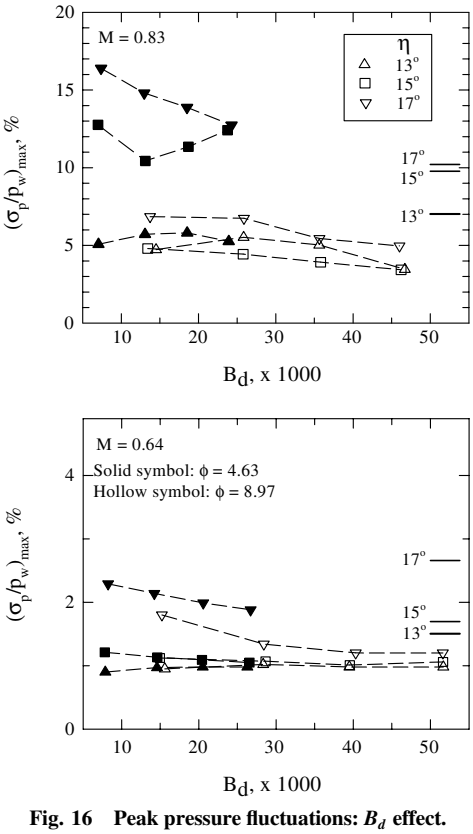

Fig. 16 Peak pressure fluctuations: B_d effect.

number. Thus, the average value of undisturbed pressure signals is employed to estimate the local peak Mach number M_1 upstream of the shock wave. In Fig. 12, it can be seen that the effect of the blowing rate is minimized for all test cases. The upstream blowing jet does not have much influence on the local Mach number near the corner in the transonic interactions. However, less expansion flows are observed for the subsonic interactions. Furthermore, the effect of the air-injection pattern is shown in Fig. 13. In general, the variation of M_1 with B_d shows a similar trend for $\phi = 4.63$ and 8.90. In the case of transition from subsonic to transonic expansion flows ($M = 0.64$ and $\eta = 17$ deg), the local peak Mach number of $\phi = 4.63$ is lower than that of $\phi = 8.90$. This is considered due to the air-injection pattern on the shape of the upstream boundary layer. It is also noted that M_1 increases slightly with increasing B_d at $M = 0.83$ (transonic interactions).

The oil-flow visualization technique is also used to visualize the surface flow pattern. A thin film of the mixture (titanium dioxide, oil, oleic acid, and kerosene) is applied on the surface of the instrumentation plate. The region of the separated boundary layer was visualized and compared with the surface-pressure measurements. In Fig. 14 (case A, plates 1 and 3 only), the upstream movement of the shock wave and a more extensively separated boundary layer (larger X_i^*) with increasing β for the baseline case can be seen [5]. With the upstream blowing jets, the shock wave location X_{sep}^* moves further upstream, particularly at higher $p_{o,j}^*$. The porosity effect is more pronounced on the extension of the separated boundary layer X_i^* for the case of initial separation ($M = 0.83$ and $\eta = 13$ deg, or $\beta \fallingdotseq 15$). For case B, the upstream blowing jets show a similar trend. The effect of the air-injection pattern is not significant.

Pressure fluctuations are coupled with global unsteadiness of the associated flow structure. In general, the shear layer structures in the buffer region are responsible for the generation of high-amplitude wall pressure peaks [21], and shock-induced separation induces peak pressure fluctuations [16]. For compressible convex-corner flows, the downstream recompression and separation of the boundary layer increase the intensity of the pressure fluctuations near the corner apex. With the upstream blowing jet, the results are shown in Fig. 15 (case A). It can be seen that the amplitude of the peak pressure fluctuation $(\sigma_p/p_w)_{\max}$ is lower than that of the baseline case. This is related to less expansion flow and the reduced adverse pressure gradient near the corner. However, the case of $\phi = 4.63$ shows an opposite trend. This is considered due to the shock excursion phenomenon. Further studies are required. It is also noted that the blowing rate has little influence in the subsonic interactions but not in the transonic interactions. In Fig. 16, the B_d effect is examined. The levels of peak pressure fluctuation for the baseline cases are shown as a solid line for each corner angle. In the subsonic interactions ($M = 0.64$ at $\eta = 13$ and 15 deg), $(\sigma_p/p_w)_{\max}$ decreases with the upstream blowing jet, and the effect of the air-injection pattern is minimized. Furthermore, more intense pressure fluctuations are observed for $\phi = 4.63$ in the transonic interactions, particularly for $M = 0.83$ at $\eta = 15$ and 17 deg. This indicates an enhanced shock oscillation.

IV. Conclusions

This paper investigates the upstream normal blowing jet on the compressible convex-corner flow in a turbulent boundary layer. Of particular interest is the study of the dependence of the blowing rate and the air-injection pattern in subsonic and transonic interactions. The apparent independence of the distributions of the mean surface pressure with the blowing rate is observed, particularly at farther downstream locations. However, there is a marked decrease in the peak Mach number (less expansive flow) in subsonic interactions. Slightly higher C_p is observed near the corner with the plate of higher porosity, and decreasing $A_{j\text{-dis}}$ induces considerably higher C_p near the corner apex. This also results in decreasing peak pressure fluctuations. For transonic interactions, the level of C_p near the corner increases with higher $p_{o,j}^*$ than that of the baseline case, and the porosity effect is not evident. The movement of peak surface-pressure fluctuations with an upstream blowing jet implies the

expansion of the separation bubble. The peak pressure fluctuations near the corner are associated with porosity and the blowing rate. Thus, the fluctuating load in the case of shock-induced boundary-layer separation would be more sensitive to an upstream disturbance.

Acknowledgments

The research was supported by the National Science Council under grant NSC 95-2212-E-006-065-MY3. The author would like to thank the technical staff of the Aerospace Science and Technology Research Center/National Cheng-Kung University for technical support with the experiments.

References

[1] Stanewsky, E., "Adaptive Wing and Flow Control Technology," *Progress in Aerospace Sciences*, Vol. 37, No. 7, 2001, pp. 583–667. doi:10.1016/S0376-0421(01)00017-3

[2] Mason, W. H., "Fundamental Issues in Subsonic/Transonic Expansion Corner Aerodynamics," AIAA Paper 93-0649, Jan. 1993.

[3] Chung, K. M., "Transition of Subsonic and Transonic Expansion-Corner Flows," *Journal of Aircraft*, Vol. 37, No. 6, 2000, pp. 1079–1082. doi:10.2514/2.2714

[4] Chung, K. M., "Unsteadiness of Transonic Convex-Corner Flows," *Experiments in Fluids*, Vol. 37, No. 6, 2004, pp. 917–922. doi:10.1007/s00348-004-0890-3

[5] Chung, K. M., "Investigation on Transonic Convex-Corner Flows," *Journal of Aircraft*, Vol. 39, No. 6, 2002, pp. 1014–1018. doi:10.2514/2.3029

[6] Inger, G. R., and Zee, S., "Transonic Shock Wave/Turbulent Boundary Layer Interaction with Suction or Blowing," *Journal of Aircraft*, Vol. 15, No. 11, 1978, pp. 750–754. doi:10.2514/3.58442

[7] Fernandez, F. L., and Zukoski, E. E., "Experiments in Supersonic Turbulent Flow with Large Distributed Surface Injection," *AIAA Journal*, Vol. 7, No. 9, 1969, pp. 1759–1767. doi:10.2514/3.5387

[8] Poggie, J., and Smits, A. J., "Shock Unsteadiness in Reattaching Shear Layer," *Journal of Fluid Mechanics*, Vol. 429, 2001, pp. 155–185. doi:10.1017/S002211200000269X

[9] Chung, K. M., "Upstream Blowing Jet on Transonic Convex Corner Flows," *Journal of Aircraft*, Vol. 44, No. 6, 2007, pp. 1948–1953. doi:10.2514/1.32203

[10] Chung, K. M., "Development and Calibration of ASTRC/NCKU 600 mm × 600 mm Transonic Wind Tunnel," National Science Council Rept. 83-2212-E-006-141T, Taipei City, Taiwan, ROC, July 1994.

[11] Gramann, R. A., and Dolling, D. S., "Detection of Turbulent-Boundary Layer Separation Using Fluctuating Wall Pressure Signals," *AIAA Journal*, Vol. 28, No. 6, 1990, pp. 1052–1056. doi:10.2514/3.25164

[12] Miau, J., Cheng, J., Chou, T., Chung, K., and Chou, J., "The Effect of Surface Roughness on the Boundary Layer Transition," *7th International Symposium in Flow Modeling and Turbulent Measurement*, National Cheng Kung Univ., Tainan, Taiwan, ROC, Oct. 1998, pp. 609–616.

[13] Vakili, A. D., Wolfe, R., Nagle, T., and Lambert, E., "Active Control of Cavity Aeroacoustics in High Speed Flows," AIAA Paper 95-0678, Jan. 1995.

[14] Ruban, A. I., Wu, X., and Pereira, R. M. S., "Viscous–Inviscid Interaction in Transonic Prandtl–Meyer Flow," *Journal of Fluid Mechanics*, Vol. 568, 2006, pp. 387–424. doi:10.1017/S0022112006002448

[15] Laganelli, A. L., and Martellucci, A., "Wall Pressure Fluctuations in Attached Boundary Layer Flows," *AIAA Journal*, Vol. 21, No. 4, 1983, pp. 495–502. doi:10.2514/3.8105

[16] Dolling, D. S., "Fifty Years of Shock-Wave/Boundary Layer Interaction Research: What Next?," *AIAA Journal*, Vol. 39, No. 8, 2001, pp. 1517–1531. doi:10.2514/2.1476

[17] Turkyilmaz, I., "An Investigation of Separation near Corner Points in Transonic Flow," *Journal of Fluid Mechanics*, Vol. 508, 2004, pp. 45–70. doi:10.1017/S0022112004008754

[18] Ruban, A. I., and Turkyilmaz, I., "On laminar Separation at a Corner Point in Transonic Flow," *Journal of Fluid Mechanics*, Vol. 423, 2000, pp. 345–380. doi:10.1017/S002211200000207X

[19] Verhoff, A., Stockesberry, D., and Michal, T., "Hodograph Solution for Compressible Flow past a Corner and Comparison with Euler Numerical Predictions," AIAA Paper 91-1547, June 1991.

[20] Alber, I. E., Bacon, J. W., Masson, B. S., and Collins, D. J., "An Experimental Investigation of Turbulent Transonic Viscid-Inviscid Interactions," *AIAA Journal*, Vol. 11, No. 5, 1973, pp. 620–627. doi:10.2514/3.50501

[21] Kim, J., Kim, K., and Sung, H., "Wall Pressure Fluctuations in a Turbulent Boundary Layer after Blowing or Suction," *AIAA Journal*, Vol. 41, No. 9, 2003, pp. 1697–1704. doi:10.2514/2.7315